Helicopter Vibration Reduction in Forward Flight Using Blade Integral Twist Actuation

SangJoon Shin*
School of Mechanical and Aerospace Engineering, Seoul National University, 56-1 Shillim-dong, Kwanak-gu, Seoul 151-744, Korea
Carlos E. S. Cesnik
Department of Aersopace Engineering, University of Michigan, 1320 Beal Ave., Ann Arbor, MI 48109, U.S.A.

An analytical framework has been developed to examine integrally-twisted helicopter blades and their aeroelastic behavior during forward flight. This is accomplished by modifying an existing multi-body dynamics code, DYMORE, with active material constitutive relations. An integral twist-actuated rotor blade was designed within this framework. A four-bladed fully-articulated active rotor system was built and tested to demonstrate the present concept in forward flight. The impact of integral twist actuation on fixed and rotating system loads during forward flight is evaluated by the proposed analysis. While discrepancies are found in the amplitude of the loads under actuation, the predicted trend of load variation with respect to its control phase correlates well with the experiments. Factors affecting the accuracy of the present analysis against the experimental results are described in detail. Based on the present discussion, an improved analysis is planned to be conducted.

Key Words : Helicopter Vibration, Integral Twist-actuated Blades, Geometrcially-exact Beam Formulation, Multi-body Dynamics, Individual Blade Control

Nomenclature

a : Global frame attached to the hub
b : Undeformed reference frame of the blade
B : Deformed reference frame of the blade
C^{ba} : Transformation matrix from a to b
C^{Ba} : Transformation matrix from a to B
C_T : Non-dimensionalized rotor thrust coefficient
F_1 : Beam axial force
$F_1^{(a)}$: actuation component of beam axial force
F_B : Internal force column vector in the B frame
$F_B^{(a)}$: Actuation column vector for internal force
$g_1(s), g_2(s), g_3(s)$: Warping due to axial strain (1) and bending strains (2, 3)
$G(s)$: Torsion related warping
H_B : Angular momentum vector in the B frame
$\mathbf{k}$: Sectional elastic curvature vector
K : Total kinetic energy of the blade
K_{ij} : Beam stiffness components
M_1, M_2, M_3 : Beam torsional moment (1) and bending moments (2,3)
$M_1^{(a)}, M_2^{(a)}, M_3^{(a)}$: Actuation component of beam torsional moment (1) and bending moments (2,3)
M_B : Internal moment column vector in the B frame
$M_B^{(a)}$: Actuation column vector for internal moment

* Corresponding Author,
E-mail : ssjoon@snu.ac.kr
TEL : +82-2-880-1642; **FAX** : +82-2-887-2662
School of Mechanical and Aerospace Engineering, Seoul National University, 56-1 Shillim-dong, Kwanak-gu, Seoul 151-744, Korea. (Manuscript **Received** June 22, 2006; **Revised** November 30, 2006)

N : Number of blades
N_{act} : Sine dwell actuation frequency in/rev
r_n : Projection of the position vector $\boldsymbol{r}$ to the vector $\boldsymbol{n}$ normal to the blade surface
P_B : Linear momentum vector in the B frame
s : Coordinate with respect to the middle surface point along the blade
u_1, u_2, u_3 : Displacement field of the cross-section reference point in the blade
$\mathbf{u}_o$: Position vector of a point on the beam reference line before deformation
$\mathbf{u}$: Position vector of a point on the beam reference line after deformation
U : Total potential energy of the blade
v_1, v_2, v_3 : Displacement of an arbitrary point in the blade
$v_1^{(a)}(s)$: Actuation to the out-of-plane displacement
$V(t)$: High voltage applied to integral actuators
$V_{amplitude}$: Amplitude of high voltage signal in volts
V_B : Linear velocity column vector in the B frame
W : External loads, such as aerodynamic force
y, z : Cartesian coordinates with respect to the reference point in the cross section
α_S : Rotor shaft tilt angle
Γ_{11} : Beam axial strain at the reference point
$\kappa_2, \kappa_2, \kappa_3$: Beam curvature due to torsion (1), and bending (2, 3) at the reference point
γ_B, κ_B : Components of sectional strain vector, measured in the B frame
$\phi(x)$: Elastic twist angle of the cross section
$\phi_{blade\ i}$: Phase difference for each i-th blade
$\phi_{control\ phase}$: Control phase for each azimuthal division
μ : Advance ratio
$\boldsymbol{\omega}$: Sectional angular velocity vector
$\omega_{actuation}$: Sine dwell actuation frequency in rad/sec
Ω : Rotor rotational frequency
Ω_B : Angular velocity column vector in the B frame
ψ : Blade azimuth angle
$(')$, $(\ )^\circ$: Derivative with respect to time
$(\ )'$: Derivative with respect to the beam spanwise coordinate, x_1

1. Introduction

Rotorcraft has been a very important means of aerial transportation due to its capability of vertical take-off and landing. However, it has also been under some serious constraints such as relatively poor ride quality when compared to their fixed wing counterparts due to high levels of vibration and noise. The primary source of vibration is the complex unsteady aerodynamic environment present around the rotor blades in forward flight. The coupling between the structural and mechanical components such as rotor, fuselage, engine, and transmission adds another degree of complexity to this problem. There have been considerable efforts in the helicopter community to reduce vibration, and most of them were based on passive methodologies (Bielawa, 1992). However, during the last two decades, active methods to alleviate helicopter vibration based on the idea of directly modifying unsteady aerodynamic loads acting upon the rotor blades have been investigated. These may be broadly classified as higher harmonic control (HHC) and individual blade control (IBC) (Shaw et al., 1989; Ham, 1987). Several outstanding results were obtained in terms of vibration reduction capability. However, these realizations are associated with employing additional hydraulic actuators installed on either non-rotating (beneath swashplate) or rotating frames (between pitch links) have not successfully entered into production vehicles.

Recently, advances in active materials have enabled multiple lightweight sensors/actuators embedded or surface-mounted at several locations in rotor blades (Loewy, 1997; Friedmann, 1997; Chopra, 2000). By employing active materials for such actuators, one can potentially obtain advantages in terms of weight and power consumption when compared with traditional hydraulic systems. Various implementations have been suggested for active materials application to the rotorcraft vibration reduction (Giurgiutiu, 2000).

Two main distinct concepts have been under development for the active material application : rotor blade flap actuation, and integral blade twist actuation. Between these, the integral twist actuation concept (Rodgers, 1998 ; Cesnik et al., 1999) is the tows of this paper. This actuation concept presents itself as an aggressive alternative with several potential benefits. The actuators once embedded in the composite construction become part of the load bearing structure, making the active blade a truly integrated multifunctional structure that allows for effective construction and assembly of future low vibration and low noise rotor blades. The integral twist actuation concept using active materials technology showed promising benefits from a conceptual standpoint (Derham and Hagood, 1996), as well as preliminary hover testing with small-scaled models (Rodgers, 1998 ; Wilbur et al., 2000). However, it was not until the open-loop wind-tunnel forward flight test (Wilbur et al., 2002) of a four-bladed Mach-scaled rotor was conducted that the fully-active concept of active twist rotor was investigated comprehensively. A series of research activities conducted previously in direct support to this test is described in detail in the relevant references : structural modeling of the integral blades (Cesnik and Shin, 2001), blade design, prototyping, and its bench test (Cesnik et al., 1999), hover test and its correlation with analysis (Wilbur et al., 2000 ; Cesnik et al., 2001), open-loop forward flight test and its correlation with analysis (Wilbur et al., 2002 ; Shin, 2001), preliminary numerical simulation of the closed-loop control (Shin, 2001), and closed-loop control test (Shin et al., 2005).

This paper focuses on the modeling of active twist rotors that were used in the development of the NASA/Army/MIT ATR blades. It describes the formulation from which forward flight simulation of the response of the helicopter rotor can be obtained, employing active composite blade with distributed anisotropic piezoelectric strain actuators. An active blade of such rotor system is analyzed in a two-step approach. First, its cross section is modeled as a multi-cell composite beam with integral anisotropic actuators (Cesnik and Shin, 2001 ; Cesnik and Morales, 2001 ; Palacios and Cesnik, 2005). Then, the cross-sectional result is used in an existing multi-body dynamics model for passive helicopter blades (Bauchau, 1998), which combines a geometrically-exact beam structural formulation and the finite-state dynamic inflow theory (Peters and He, 1995). Results from the open-loop forward flight experiment are correlated with the prediction from the simulation.

2. Analytical Framework

For analyzing helicopter blades with embedded strain actuators, a framework is needed such that the effects of the active material embedded in the structure are carried out throughout all the steps of the analysis. Since there were no analysis formulations available which could properly handle all the peculiarities of an active helicopter blade cross section, the authors have created a general framework for active rotor blade modeling. Here, an asymptotical analysis takes the electromechanical three-dimensional problem and reduces it into a set of two analyses : a linear analysis over the cross section and a nonlinear analysis of the resulting beam reference line. By coupling the active blade formulation with the appropriate un-

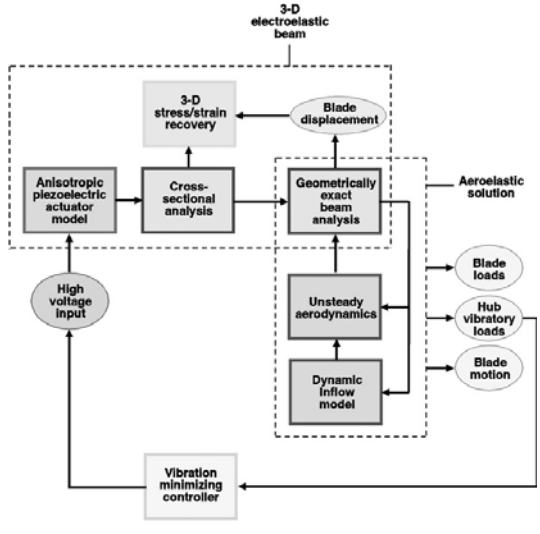

Fig. 1 Schematic diagram of the analytical framework for an active helicopter blade and its aeroelastic behavior

steady aerodynamics, the aeroelastic problem can then be solved in time and simulations be conducted for control design. A schematic diagram of the established framework is shown in Fig. 1.

2.1 Cross-sectional analysis

An analytic formulation for a two-cell thin-walled composite beam with integral anisotropic piezoelectric actuators was derived to design and analyze an active twist helicopter rotor blade (Cesnik and Shin, 2001). It is an asymptotically correct formulation stemming from shell theory. While restricted to thin-walled beams, it yielded closed form solutions of the displacement field (which was derived and not assumed), and stiffness and actuation constants. The availability of correct closed form expressions was essential to determine design paradigms on this new type of blade, mainly concerning to the tradeoffs between torsional stiffness and twist actuation. These stiffness and actuation constants are then used in a beam finite element discretization of the blade reference line. With an assumed linear piezoelectric constitute relation and starting from a shell strain energy, the 2-D original electroelastic shell formulation is condensed to a 1-D beam problem. The displacement field was found to be:

$$\begin{aligned} v_1 &= u_1(x) - y(s)\,u_2'(x) - z(s)\,u_3'(x) \\ &\quad + G(s)\,\phi'(x) + g_1(s)\,u_1'(x) \\ &\quad + g_2(s)\,u_2''(x) + g_3(s)\,u_3''(x) + v_1^{(a)}(s) \\ v_2 &= u_2(x)\frac{dy}{ds} + u_3(x)\frac{dz}{ds} + \phi(x)\,r_n \\ v_3 &= u_2(x)\frac{dz}{ds} - u_3(x)\frac{dy}{ds} - \phi(x)\,r_n \end{aligned} \tag{1}$$

where the superscript (a) indicates that the component is function of the applied electric field (in the case of thin-walled cross sections, the actuation only influences the out-of-plane component of the displacement field). The functions $G(s)$ and $g_i(s)$ are the warping functions associated with torsion, extension, and two bending measures. Associated with this displacement field, the beam constitutive relation relating beam generalized forces (axial force, twist, and two bending moments, respectively) with beam generalized strains (axial strain, twist curvature, and two bending curvatures) and corresponding generalized actuation forces (function of the geometry, material distribution, and applied electric field) was obtained in the following form:

$$\begin{Bmatrix} F_1 \\ M_1 \\ M_2 \\ M_3 \end{Bmatrix} = \begin{bmatrix} K_{11} & K_{12} & K_{13} & K_{14} \\ K_{12} & K_{22} & K_{23} & K_{24} \\ K_{13} & K_{23} & K_{33} & K_{34} \\ K_{14} & K_{24} & K_{34} & K_{44} \end{bmatrix} \begin{Bmatrix} \gamma_{11} \\ \kappa_1 \\ \kappa_2 \\ \kappa_3 \end{Bmatrix} - \begin{Bmatrix} F_1^{(a)} \\ M_1^{(a)} \\ M_2^{(a)} \\ M_3^{(a)} \end{Bmatrix} \tag{2}$$

where $[K]$ is the stiffness matrix function of geometry and material distribution at the rotor cross section. From this formulation, all K_{ij} and the generalized actuation forces are given by closed form expressions (Cesnik and Shin, 2001).

2.2 1-D beam structural and aerodynamic analyses

To simulate the active twist rotor system, a time domain formulation is needed. The multi-body dynamics code DYMORE, developed by Bauchau (1998), is based on the geometrically-exact beam equations and it is coupled to the aerodynamics of Peters and He (1995). DYMORE's original beam formulation is consistent with the one used previously by the authors in investigating the hover response of the active rotor system (Cesnik et al., 2001). The difference is that the DYMORE's formulation is a displacement-based form instead of the mixed-form. Therefore, the cross-sectional analysis developed by the authors for active beams, Eq. (2), is incorporated in DYMORE in this paper. The integral actuation forces and moments existing inside the blade structure are realized in the form of finite element loads to the passive beam in the presently modified new version of DYMORE. In what follows, the modifications to the existing formulations of DYMORE for the present active beam analysis are briefly described.

The kinetic and strain energies of the beam are expressed as follows

$$\begin{aligned} K &= \frac{1}{1}\int_0^L \begin{Bmatrix} V_B \\ \Omega_B \end{Bmatrix}^T \begin{Bmatrix} P_B \\ H_B \end{Bmatrix} dx_1 \\ U &= \frac{1}{2}\int_0^L \begin{Bmatrix} \gamma_B \\ \kappa_B \end{Bmatrix}^T \begin{Bmatrix} F_B \\ M_B \end{Bmatrix} dx_1 \end{aligned} \tag{3}$$

where K and U are the kinetic and potential energies of the beam, F_B and M_B internal force and

moment column vectors, P_B and H_B linear and angular momentum column vectors, V_B and Ω_B linear and angular velocity column vectors, γ_B and κ_B the generalized strain column vectors, respectively. The quantities with the subscript B means those under the deformed beam configuration. The velocity-displacement and strain-displacement relationships are described as

$$\begin{Bmatrix} V_B \\ \Omega_B \end{Bmatrix} = \begin{bmatrix} (C^{ba})^T (C^{Bb})^T \dot{\mathbf{u}} \\ (C^{ba})^T (C^{Bb})^T \boldsymbol{\omega} \end{bmatrix}$$
$$\begin{Bmatrix} \gamma_B \\ \kappa_B \end{Bmatrix} = \begin{bmatrix} (C^{ba})^T (C^{Bb})^T (\mathbf{u}_o' + \mathbf{u}') - \mathbf{1} \\ (C^{ba})^T (C^{Bb})^T \mathbf{k} \end{bmatrix} \quad (4)$$

where the superscripts b, B, and a mean the undeformed, deformed and the inertial beam frames of reference, and the matrices C with the appropriate superscripts are the direction cosine matrices signifying the transformation among those frames. ω is the sectional angluar velocity vector; $\mathbf{u}_o$ defines the position of a point on the reference line before deformation, measured in a frame; $\mathbf{u}$ defines the displacement of a point to the deformed configuration, meaured in a frame; and $\mathbf{k}$ is the sectional elastic curvature vector. The dot means a derivative with respect to time and the prime with respective to the beam reference line x_1. The relations presented in Eq. (4) are geometrically exact, which means that they are valid for arbitrarily large displacements and rotations, although the strains are assumed to be small. The equations of motion for the beam are derived from Hamilton's principle, such as

$$\int_{t_i}^{t_f} [\delta(K+U) + \delta W] dt = 0 \quad (5)$$

where δW is the variation of the virtual work done by the externally applied loads, such as aerodynamic forces. By incorporating Eq. (3), one obtains

$$\int_{t_i}^{t_f} \left[\begin{Bmatrix} \delta V_B \\ \delta \Omega_B \end{Bmatrix}^T \begin{Bmatrix} P_B \\ H_B \end{Bmatrix} - \begin{Bmatrix} \delta \gamma_B \\ \delta \kappa_B \end{Bmatrix}^T \begin{Bmatrix} F_B \\ M_B \end{Bmatrix} + \delta W \right] dt = 0 \quad (6)$$

The sectional internal forces are now substituted with the constitutive relation, Eq. (2), which is suggested by the authors, considering the existence of the actuation forcing vector. The sectional momenta is also represented by an appropriate inertial matrix as well. Substituting Eqs. (2) and (4) into (6), and integrating by parts yield the governing simultaneous equations as follows.

$$\begin{aligned} &(C^{Bb}C^{ba}P_B)^{\cdot} - (C^{Bb}C^{ba}F_B)' = \hat{\mathbf{q}} + (C^{Bb}C^{ba}F_B^{(a)})' \\ &(C^{Bb}C^{ba}H_B)^{\cdot} - \tilde{\mathbf{u}}^T C^{Bb}C^{ba}P_B - (C^{Bb}C^{ba}M_B)' \\ &+ (\mathbf{u}_o' + \mathbf{u}')^T C^{Bb}C^{ba}F_B \\ &= \breve{\mathbf{q}} - (C^{Bb}C^{ba}M_B^{(a)})' + (\mathbf{u}_o' + \mathbf{u}')^T C^{Bb}C^{ba}F_B^{(a)} \end{aligned} \quad (7)$$

where $\mathbf{q}^T = [\hat{\mathbf{q}}^T \ \breve{\mathbf{q}}^T]$ are the externally applied loads per unit span length, measured in a frame. As desribed earlier, the effect of the actuation forcing vector is treated as an additional external load in the right-hand side of Eq. (7). This is a new formulation obtained and used in the present paper to analyze the behavior of the active blades in forward flight condition. In the previous formulation obtained for the bench and hover analysis, the effect of actuation forcing vectors remained as an auxillary form to reinforce the generalized strain variables. (Cesnik et al., 2001) The solution of the present 1-D beam analysis provides blade displacement and generalized stress fields due to external loading and piezoelectric actuation, which are of interest in the analysis of static and dynamic deformations and aeroelastic stability.

The forward flight part of the finite-state dynamic inflow aerodynamics model (Peters and He, 1995) is constructed by applying the acceleration potential theory to the rotor aerodynamics problem with a skewed cylindrical wake. More specifically, the induced flow at the rotor disk is expanded in terms of modal functions. As a result, a three-dimensional, unsteady induced-flow aerodynamics model with finite number of states is derived in time domain. This model falls on an intermediate level of wake representation between the simplest momentum and the most complicated free wake methodologies. It does not require an intense computational effort, and it is applicable to the problems of rotor aeroelastic stability, basic blade-passage vibrations, and higher-harmonic control studies.

2.3 Aeroelastic system in forward flight

The aeroelastic system of equations that combines the structural and aerodynamic equations obtained in the previous steps is now solved for

forward flight transient response. Specifically, the present analysis adopts a direct time integration of the blade response due to integral actuation during flight. DYMORE adopts a time-discontinuous integration scheme with energy decaying characteristics in order to avoid high frequency numerical oscillation (Bauchau, 1998). Such an adverse high frequency oscillation usually occurs during a finite element time integration of a complex multi-body dynamic system. Finally, variation of the hub shear vibratory loads at N/rev (or NP) frequency due to blade twist actuation can be calculated by Fourier transform of the time response of either the blade or the entire active rotor system for different forward flight conditions.

2.4 Prescribed twist actuation signal for individual blade control

The forward flight regime is of great interest for the vibration reduction problem. The blade twist actuation is suggested to alter the undesirable unsteady aerodynamic environment which develops in that flight regime. Once the steady-state equilibrium condition is obtained by adjusting blade pitch control, either sine-dwell or sine-sweep high-voltage signal is applied to the embedded actuators. In case of sine-dwell signal, only 3P, 4P, 5P frequency components are considered since $(N-1, N, N+1)$ frequency components are found to influence significantly N-bladed rotor system. Two blade control modes are tested: collective twist and an Individual Blade Control (IBC), where all the blades have the same twist actuation variation with azimuth. Experimentally, the collective mode was found to be relatively ineffective in altering fixed-system vibratory loads compared with the IBC mode (Wilbur et al., 2002). The correlations presented in this paper will concentrate on those obtained during the simulated 1 g level flight conditions while in the baseline (no actuation) and IBC mode of actuation. Also, a sweeping algorithm over control phase angle is considered within the IBC scheme.

Three modes of blade actuation were considered in the forward flight open-loop control experiment. In order to efficiently impose an IBC-mode sine-dwell signal with control phase variation, a series of high-voltage input is generated using the following formula

$$V(t) = V_{amplitude} \times \cos\{2\pi\omega_{actuaion}(t-\phi_{control\_phase}) + 2N_{act}\pi\cdot\phi_{blade\_i}\} \quad (8)$$

where,

$V_{amplitude}$=500, 750, or 1,000 V
$\omega_{actuation}=N_{act}\times f_{rotation}$
$\phi_{control\_phase}$=0, 0.8, ⋯, 1.0
(12 divisions over 360°)
N_{act}=3, 4, or 5
ϕ_{blade_i}=0 (Blade No. 1), 0.25 (Blade No. 2), 0.5 (Blade No. 3), 0.75 (Blade No. 4)

An example of the high-voltage input signal

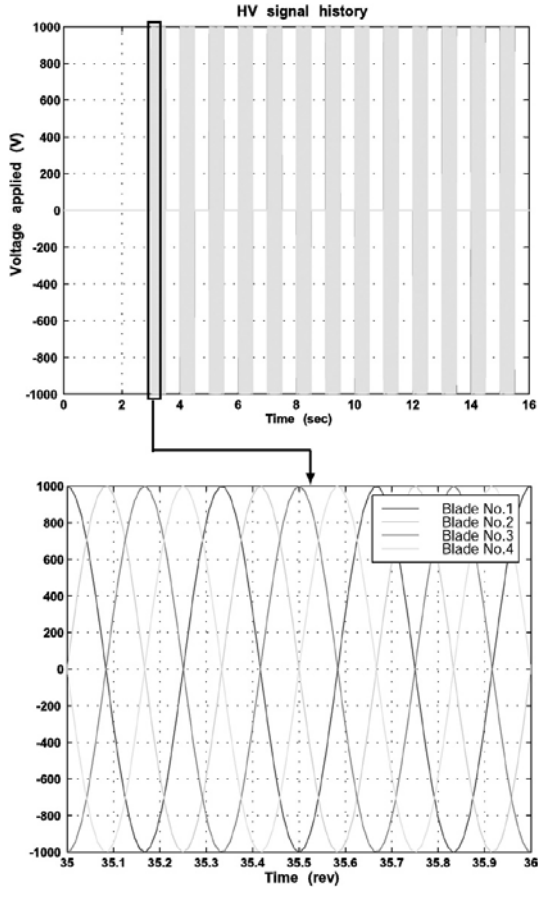

Fig. 2 Example of high-voltage input generated for an IBC-mode 3P actuation with 12 divisions control phase angle

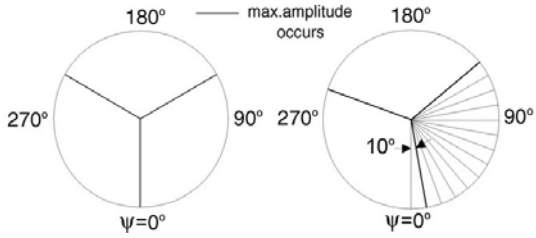

Fig. 3 Azimuthal locations where the maximum amplitude occurs for the first two actuation periods during the 3P actuation input generated in Fig. 2

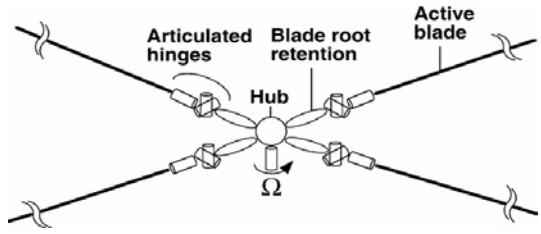

Fig. 4 Detailed multibody representation of 4-active-bladed ATR system

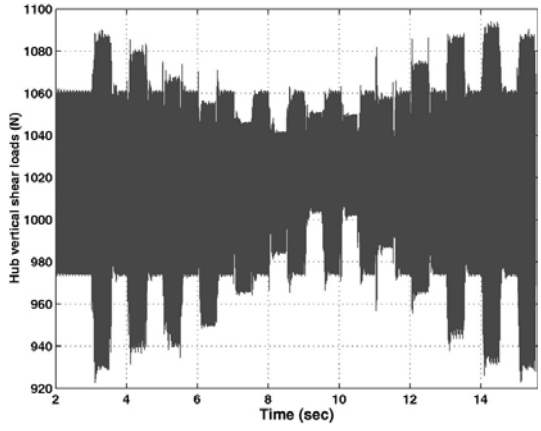

Fig. 5 Simulated time history of hub vertical shear forces when the 3P actuation is applied as described in Fig. 2

generated for an IBC-mode 3P actuation with 12 divisions of control phase angle is shown in Fig. 2. No actuation is applied for the initial 3 seconds to establish a steady-state equilibrium for the given flight condition. At the same time, the baseline (no actuation) quantities are extracted during the last period of this interval, say between 2.5 and 3.0 s, to be compared with those under actuation. Then, for each 0.5-s period of actuation, each with different control phase angle, another 0.5-s period of no actuation exists between them. These are applied one after the other as shown in Fig. 2. By applying this control phase algorithm, the blades exhibit the maximum amplitudes of the sinusoidal electric field at certain azimuthal locations as exemplified in Fig. 3. The maximum amplitude occurrence during the first and second actuation periods shows an azimuthal difference of 10° corresponding to 120°/12 divisions, although it is designated as a phase difference of 30° corresponding to 360°/12 divisions in terms of control phase.

3. Open-Loop Forward Flight Results

3.1 Results of fixed and rotating system loads

Figure 4 shows a model of the four-active-bladed ATR system used in present analysis. The hub reaction loads of the rotor system can be obtained from summation of all the loads in the four root retention elements at root location. Fig. 5 shows the simulated vertical component of the hub shear forces developed in the system when 3P sine-dwell actuation is applied as described in Fig. 2. The steady-state trim condition is $\mu=0.333$, $\alpha_S=-6°$, $C_T=0.0066$. As one can observe from Fig. 5, there is a considerable change in the magnitude of the vibratory loads for certain control phase actuation. The highest reduction happens in the interval of 9 to 9.5 s and 10 to 10.5 s. These time domain quantities can be transferred to frequency domain to examine the magnitude of the frequency content of interest, which is 4P in the four-bladed rotor system. Results are shown in Fig. 6 with the corresponding experimental data for 3P, 4P, 5P actuation applied during the same steady-state trim condition. In the figures, the lines are simple interpolation of the solution points which are obtained from the analysis at discretely increased control phase, while the experimental data are still displayed with the discrete symbols.

The load predicted from the analysis shows significant discrepancy in amplitude from the

experimental results, although their variation trends in terms of control phase are in good agreement. 3P actuation is most effective in hub shear vibratory load reduction, resulting in 95% reduction. Such a hub shear vibratory load reduction performance numerically predicted here shows similar trend as it was observed in the experiment. Quantities in the rotating-system, for example, flap bending moment, are also shown in Fig. 7. The span location where these quantities are calculated is selected to match those of the strain gauges embedded in the test blade. While the fixed-system quantities were investigated only in 4P frequency components, those in the rotating-system are extracted and examined in their 3P, 4P, and 5P frequency components.

Both of fixed and rotating system predicted loads exhibit significant discrepancy in amplitude from the experimental results. Since the dynamics of the test apparatus used for the wind-tunnel test is not included in the model, this may be responsible for some of the discrepancies. Upgraded input model for the same rotor system including the

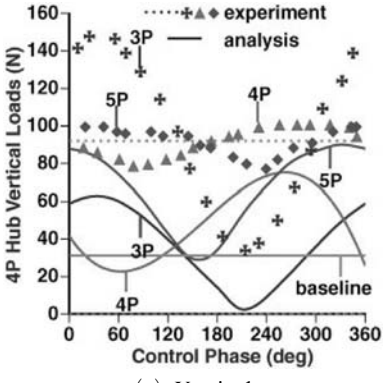

(a) Vertical

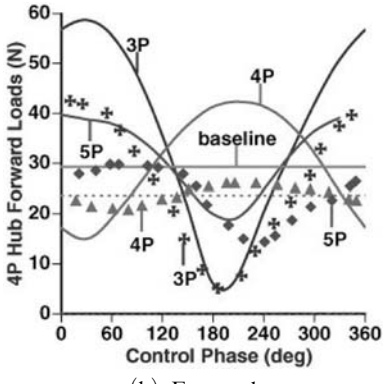

(b) Forward

Fig. 6 Variation of 4P hub shear vibratory loads for μ=0.140, α_S=−1°, C_T=0.0066, and 1,000 V twist actuation at 3P, 4P, 5P

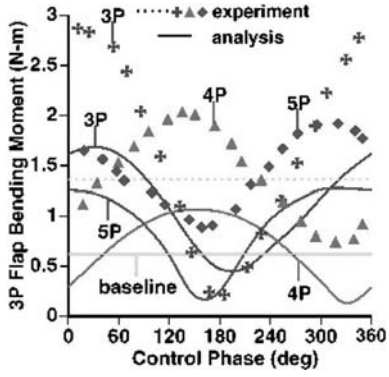

(a) 3P loads

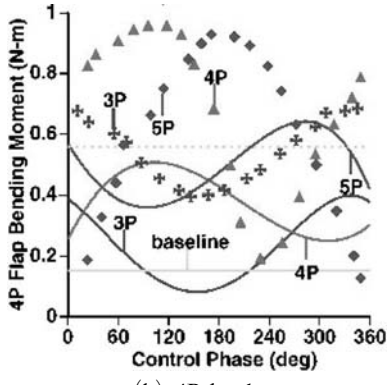

(b) 4P loads

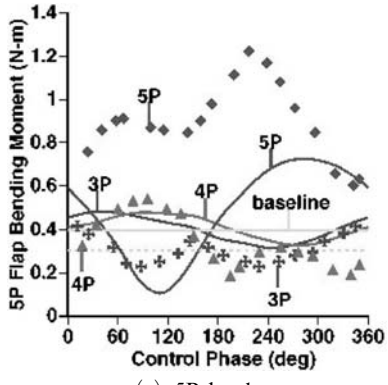

(c) 5P loads

Fig. 7 Variation of flap moments 28.7% span loation for μ=0.140, α_S=−1°, C_T=0.0066, and 1,000 V twist actuation at 3P, 4P, 5P with respect to control phase angle

pitch link and all the linkage components in the swashplate is attempted for better correlation as described in next section.

4. Improved Analysis Results

4.1 Upgraded model with detailed components

The upgraded input model including the detailed components is depicted in Fig. 8, where the pitch link mechanism is displayed only for one blade for convenience. Most newly included components are modeled as rigid bodies, reflecting the fact that the experimental rotor system is extremely stiff compared with the practical helicopter fuselage and components. However, the pitch link and rotor shaft are modeled as elastic beam, where the pitch link dynamics is specified with a stiffness value that represents the flexibility of the whole control system. By including the pitch link mechanism in the model, the pitch/flap coupling existing in the test apparatus, which amounts to 0.5 in flap up/leading edge down fashion, is implemented.

4.2 Results of fixed and rotating system loads

The same IBC-mode sine-dwell signal generated in the previous section is applied in the upgraded analysis model, and both fixed- and rotating-system loads are recorded during the simulation. By processing the time domain results in the same way as in the previous section, corresponding frequency domain components are obtained. These are shown in Figs. 9-10 together with the experimental data and the analytical results previously obtained from the one without pitch link. A correlation on the pitch link load is possible for the current upgraded model, and shown in Fig. 11.

However, such increase in model detail has shown little impact on the load prediction. Most of all, the discrepancies regarding the baseline load prediction are hardly corrected by the model upgrade. Thus, it is briefly concluded that the sources from which the present discrepancies originate are still not properly included in the

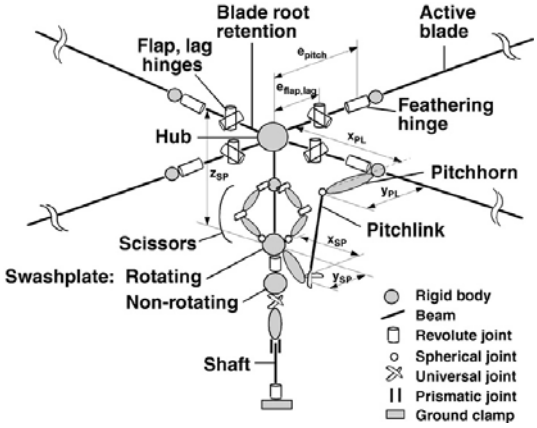

Fig. 8 Upgraded input model of the rotor system including pitch link and swashplate components

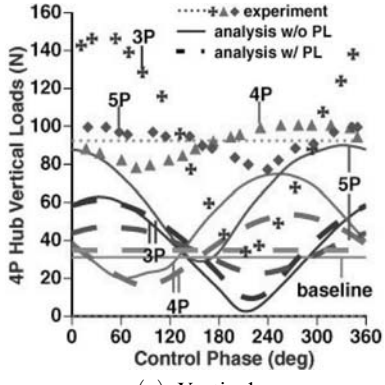

(a) Vertical

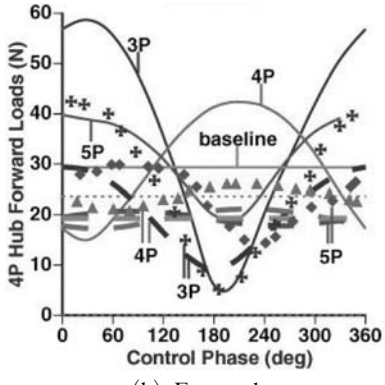

(b) Forward

Fig. 9 Variation of 4P hub shear vibratory loads for μ=0.140, α_S=−1°, C_T=0.0066, and 1,000 V twist actuation at 3P, 4P, 5P with respect to control phase angle: experiment, analysis without pitch link, and analysis with pitch link

upgraded model analysis. Sources of the discrepancies between analysis and experiment are carefully addressed and discussed in the following section. Although the previous model is crude in its representation of the swashplate control system, it is capable of exhibiting similar details on

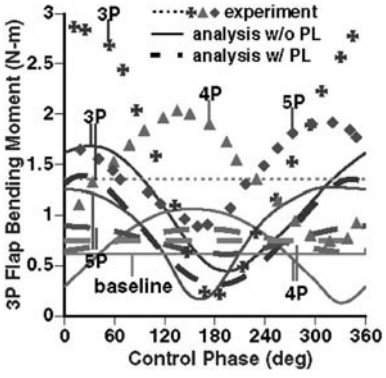

(a) 3P loads

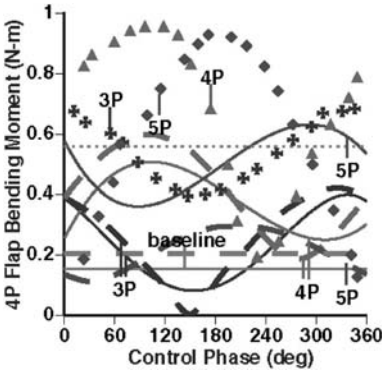

(b) 4P loads

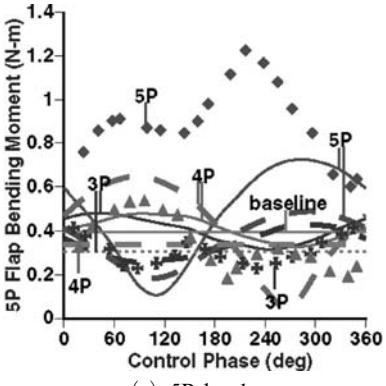

(c) 5P loads

Fig. 10 Variation of flap moments 28.7% span loation for μ=0.140, α_S=−1°, C_T=0.0066, and 1,000 V twist actuation at 3P, 4P, 5P with respect to control phase angle : experiment, analysis without pitch link, and analysis with pitch link

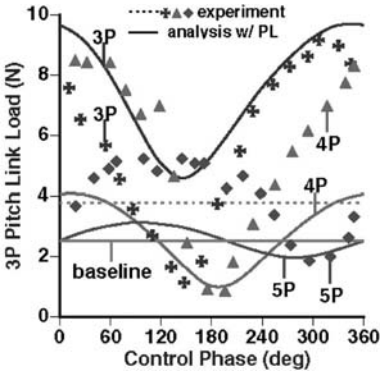

(a) 3P loads

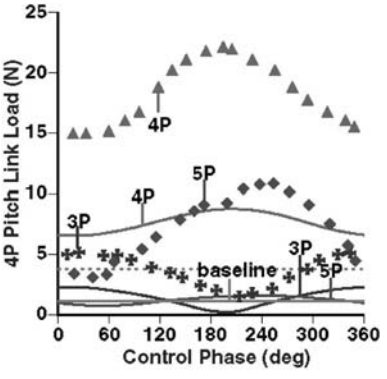

(b) 4P loads

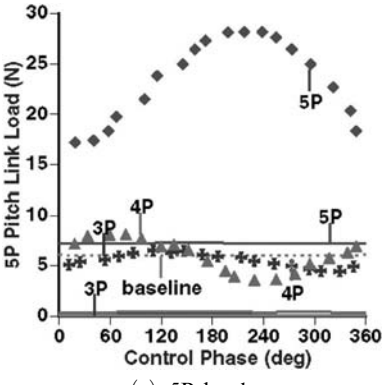

(c) 5P loads

Fig. 11 Variation of the pitch link axial load for μ=0.140, α_S=−1°, C_T=0.0066, and 1,000 V twist actuation at 3P, 4P, 5P with respect to control phase angle : experiment and analysis with pitch link

the dynamic characteristics of the ATR system with much lower computational effort.

4.3 Discussion

Both of fixed- and rotating-system loads predicted from the present two analyses exhibit significant discrepancy in amplitude from the experimental results, although their variation trend in terms of control phase is in good agreement. It should be further noted that the baseline amplitude in most of the cases are significantly underpredicted by the numerical analysis.

An extra investigation to improve the correlation on the baseline load amplitude is conducted first. For the analysis model without pitch link, blade structural modeling accuracy is examined with respect to the evaluated stiffness matrix and chordwise c.g. location, which are regarded as factors affecting the dynamics of the rotor system. According to the blade cross-sectional analysis, it is found that the present ATR test blade has its chordwise c.g. at 18% location, although the blade manufacturers usually suggest that it be 25% location. Also, the analysis indicates that the shear center is located at 30% chord instead of the 25% chord that coincides with the blade reference line. This effect can be included in the analysis by simply using the fully-populated stiffness matrix. Therefore, different models of the ATR dynamics are now constructed and the new prediction on the baseline loads are obtained for the forward flight condition, as shown in Table 1. Variations in the load prediction are observed from the various structural modeling. However, these variations do not significantly improve the correlation with the experiments. Among them, the model with pitch link does exhibit a slight improvement even with a crude structural modeling for the blade. Therefore, an analysis model with a diagonal stiffness representation, 30% shear center, and 25% c.g. location is selected as a possible candidate for further investigation to diminish the discrepancies between analysis and experiment.

Also, the experimental 4P hub sideward baseline force (See Table 1) exhibits an unreasonably high magnitude when compared to the other two hub force components. This suggests that further characterization of the entire experimental apparatus is desirable. When such characterization is completed and the detailed information is brought into the analysis model, an improved correlation between them is anticipated. In this paper, preliminary active aeroelastic characteristics of the ATR system are captured solely by analysis, and reinforcement by the experimental result will be conducted in the future.

There exist other factors which may influence the accuracy of both analysis and experiment. In the analysis, the predicting accuracy is influenced by the aerodynamics model used. As described earlier, the one adopted in the present analysis is considered to be accurate enough for the general rotor aeroelasticity investigation. However, it is recently found that a more sophisticated wake model, such as free wake model, is especially needed for an accurate estimation of the rotor system load, especially in the case of higher harmonic control (van der Wall, 2000). Also, it is also suggested that the present aerodynamics be reinforced by an appropriate dynamic stall model, which is not included in the present implementation.

Table 1 Fixed-system baseline loads predicted with different blade structural representations and c.g. locations (μ=0.140, α_S=−1°, C_T=0.0066)

	Stiffness matrix representation	Chordwise c.g. (%)	Baseline loads (N)		
			Vertical	Forward	Sideward
Model without pitch link	diagonal	25	31.1	29.3	15.3
	diagonal	18	14.1	10.6	3.6
	Fully-populated	18	19.4	16.1	4.5
Model with pitch link	diagonal	25	34.8	29.3	36.9
Experiment	—	—	92.0	23.6	142.8

In the experiment, noise induced in the instrumentation may be a significant degrading factor on the accuracy of the result. In the present experimental data, instrumentation noise is manifested in the rotating-system loads measurement. For example, flap bending strain gauge measurements show irregular variation in Fig. 7(c). Also, recirculation inside the wind tunnel may contribute to variations in the blade response, even though this effect has been considered to be small by the engineers at NASA Langley, based on previous experiments using the same test setup.

5. Conclusions

This paper addresses helicopter vibration reduction using integral blade twist control. A numerical aeroelastic framework is proposed for this study. For its implementation, an existing multi-body dynamics code, DYMORE, is modified to account for the distributed anisotropic piezocomposite actuators. The analytical results of open-loop IBC-mode actuation is correlated with the experimental data collected in wind tunnel test. While discrepancies are found in the amplitude of the loads under actuation, the predicted trend of load variation with respect to its control phase correlates well with the experiments. Among the actuation signals used, 3P IBC mode shows most effective reduction in hub shear vibratory loads at a certain control phase angle, by approximately 95%. Better correlation is attempted with upgraded analysis model, but significant improvement is not obtained.

Acknowledgments

This work is supported by the Korean Research Foundation Grant funded by the Korean Government (MOEHRD) (KRF-2006-209-D00001), and also by the Grant No. R01-2005-10059-0 from the Basic Research Program of the Korea Science and Engineering Foundation.

References

Bauchau, O. A., 1998, "Computational Schemes for Flexible, Nonlinear Multi-Body Systems," *Multi-body Dynamics*, Vol. 2, pp. 169～225.

Bielawa, R., 1992, *Rotary Wing Structural Dynamics and Aeroelasticity*, American Institute of Aeronautics and Astronautics.

Cesnik, C. E. S., Shin, S. J., Wilkie, W. K., Wilbur, M. L. and Mirick, P. H., 1999, "Modeling, Design, and Testing of the NASA/Army/MIT Active Twist Rotor Prototype Blade," *American Helicopter Society 55th Annual Forum*, Montreal, Canada.

Cesnik, C. E. S. and Shin, S. J. 2001, "On the Modeling of Integrally Actuated Helicopter Blades," *International Journal of Solids and Structures*, Vol. 38, No. 10-13, pp. 1765～1789.

Cesnik, C. E. S., Shin, S. J. and Wilbur, M. L., 2001, "Dynamic Response of Active Twist Rotor Blades," *Smart Materials and Structrues — Special Issue on Rotorcraft Application*, Vo. 10, pp. 62～76.

Cesnik, C. E. S. and Ortega-Morales, M., 2001, "Active Beam Cross-Sectional Modeling," *Journal of Intelligent Material Systems and Structures*, Vol. 12, No. 7, pp. 483～496.

Chopra, I., 2000, "Status of Application of Smart Structures Technologies to Rotorcraft Systems," *Journal of the American Helicopter Society*, Vol. 45, No. 4, pp. 228～252.

Derham, R. and Hagood, N., 1996, "Rotor Design Using Smart Materials to Actively Twist Blades," *American Helicopter Society 52nd Annual Forum*, Vol. 2, pp. 1242～1252, Washington, D.C.

Friedmann, P. P., 1997, "The Promise of Adaptive Materials for Alleviating Aeroelastic Problems and Some Concerns," *the Innovation in Rotorcraft Technology*, London, United Kingdom.

Giurgiutiu, V., 2000, "Recent Advances in Smart Material Rotor Control Actuation," *AIAA/ASME/ASCE/AHS/ASC 41st Structures, Structural Dynamics and Materials Conference*, AIAA Paper No. 2000-1709, Atlanta, GA.

Ham, N. D., 1987, "Helicopter Individual-Blade-Control Research at MIT 1977-1985," *Vertica*, Vol. 11 No. 1/2, pp. 109～122.

Loewy, R., 1997, "Recent Developments in Smart Structures with Aeronautical Applications," *Smart*

Materials and Structures, Vol. 6, pp. 11～42.

Palacios, R. and Cesnik, C. E. S., 2005, "Cross-Sectonal Analysis of Non-homogeneous Anisotrpic Active Slender Structures," *AIAA Journal*, Vol. 43, No.12, pp. 2624～2638.

Peters, D. A. and He, C. J., 1995, "Finite State Induced Flow Models Part II : Three-Dimensional Rotor Disk," *Journal of Aircraft*, Vol.32, No. 2, pp. 323～333.

Rodgers, J. P. and Hagood, N. W., 1998, "Development of an Integral Twist-Actuated Rotor Blade for Individual Blade Control," Active Materials and Structures Laboratory, Massachusetts Institute of Technology, AMSL Report #98-6, Cambridge, MA.

Shaw, J., Albion N., Hanker E. J. and Teal, R. S., 1989, "Higher Harmonic Control : Wind Tunnel Demonstration of Fully Effective Vibratory Hub Force Suppression," *Journal of the American Helicopter Society*, Vol. 31, No. 1, pp. 14～25.

Shin, S. J. and Cesnik, C. E. S., 1999, "Design, Manufacturing and Testing of an Active Twist Rotor," AMSL Report #99-3, Active Materials and Structures Laboratory, Massachusetts Institute of Technology.

Shin, S. J. and Cesnik, C. E. S., 2001a, "Forward Flight Response of the Active Twist Rotor for Helicopter Vibration Reduction," *AIAA/ASME/ASCE/AHS/ASC 42nd Structures, Structural Dynamics and Materials Conference*, AIAA Paper No. 2001-1357, Seattle, WA.

Shin, S. J. and Cesnik, C. E. S., 2001b, "Integral Twist Actuation of Helicopter Rotor Blades for Vibration Reduction," AMSL Report #01-07, Active Materials and Structures Laboratory, Massachusetts Institute of Technology.

van der Wall, B. G., 2000, "Simulation of HHC on Helicopter BVI Noise Emission Using a Prescribed Wake Method," *26th European Rotorcraft Forum*, Hague, Netherlands.

Wilbur, M. L., Yeager, W. T., Jr., Wilkie, W. K., Cesnik, C. E. S. and Shin, S. J., 2000, "Hover Testing of the NASA/Army/MIT Active Twist Rotor Prototype Blade," *American Helicopter Society 56th Annual Forum*, Virginia Beach, VA.

Wilbur, M. L., Mirick, P. H., Yeager, W. T., Jr., Langston, C. W., Cesnik, C. E. S. and Shin, S. J., 2002, "Vibratory Loads Reduction Testing of the NASA/Army/MIT Active Twist Rotor," *Journal of the American Helicopter Society*, Vol. 47, No. 2, pp. 123～133.